Laser excitation of the $n = 3$ level of positronium for antihydrogen production

S. Aghion,[1,2] C. Amsler,[3] A. Ariga,[3] T. Ariga,[3] G. Bonomi,[4,5] P. Bräunig,[6] J. Bremer,[7] R. S. Brusa,[8,9] L. Cabaret,[10] M. Caccia,[2,11] R. Caravita,[12,13] F. Castelli,[2,14] G. Cerchiari,[15] K. Chlouba,[16] S. Cialdi,[2,14] D. Comparat,[10] G. Consolati,[1,2] A. Demetrio,[6] L. Di Noto,[12,13] M. Doser,[7] A. Dudarev,[7] A. Ereditato,[3] C. Evans,[1,2] R. Ferragut,[1,2] J. Fesel,[7] A. Fontana,[5] O. K. Forslund,[7] S. Gerber,[7] M. Giammarchi,[2,3] A. Gligorova,[17] S. Gninenko,[18] F. Guatieri,[8,9] S. Haider,[7] H. Holmestad,[19] T. Huse,[19] I. L. Jernelv,[7] E. Jordan,[15] A. Kellerbauer,[15] M. Kimura,[3] T. Koettig,[7] D. Krasnicky,[12,13] V. Lagomarsino,[12,13] P. Lansonneur,[23] P. Lebrun,[23] S. Lehner,[20] J. Liberadzka,[7] C. Malbrunot,[7,20] S. Mariazzi,[20,*] L. Marx,[7] V. Matveev,[18,21] Z. Mazzotta,[2,14] G. Nebbia,[22] P. Nedelec,[23] M. Oberthaler,[6] N. Pacifico,[17] D. Pagano,[4,5] L. Penasa,[8,9] V. Petracek,[16] C. Pistillo,[3] F. Prelz,[2] M. Prevedelli,[24] L. Ravelli,[8,9] L. Resch,[7] B. Rienäcker,[7] O. M. Røhne,[19] A. Rotondi,[5,25] M. Sacerdoti,[2,14] H. Sandaker,[19] R. Santoro,[2,11] P. Scampoli,[3,26] L. Smestad,[7,27] F. Sorrentino,[12,13] M. Spacek,[16] J. Storey,[3] I. M. Strojek,[16] G. Testera,[13] I. Tietje,[7] S. Vamosi,[20] E. Widmann,[20] P. Yzombard,[10] J. Zmeskal,[20] and N. Zurlo[5,28]

(AEgIS Collaboration)

[1]*Politecnico of Milano, Piazza Leonardo da Vinci 32, 20133 Milano, Italy,*

[2]*Istituto Nazionale di Fisica Nucleare Milano, via Celoria 16, 20133 Milano, Italy*

[3]*Laboratory for High Energy Physics, Albert Einstein Center for Fundamental Physics, University of Bern, 3012 Bern, Switzerland*

[4]*Department of Mechanical and Industrial Engineering, University of Brescia, via Branze 38, 25123 Brescia, Italy*

[5]*Istituto Nazionale di Fisica Nucleare Pavia, via Bassi 6, 27100 Pavia, Italy*

[6]*Kirchhoff-Institute for Physics, Heidelberg University, Im Neuenheimer Feld 227, 69120 Heidelberg, Germany*

[7]*Physics Department, CERN, 1211 Geneva 23, Switzerland*

[8]*Department of Physics, University of Trento, via Sommarive 14, 38123 Povo, Trento, Italy*

[9]*TIFPA/Istituto Nazionale di Fisica Nucleare Trento, via Sommarive 14, 38123 Povo, Trento, Italy*

[10]*Laboratoire Aimé Cotton, Université Paris-Sud, ENS Cachan, Centre National de la Recherche Scientifique, Université Paris-Saclay, 91405 Orsay Cedex, France*

[11]*Department of Science, University of Insubria, Via Valleggio 11, 22100 Como, Italy*

[12]*Department of Physics, University of Genova, via Dodecaneso 33, 16146 Genova, Italy*

[13]*Istituto Nazionale di Fisica Nucleare Genova, via Dodecaneso 33, 16146 Genova, Italy*

[14]*Department of Physics, Universitá degli studi di Milano, via Celoria 16, 20133 Milano, Italy*

[15]*Max Planck Institute for Nuclear Physics, Saupfercheckweg 1, 69117 Heidelberg, Germany*

[16]*Czech Technical University, Prague, Bøehová 7, 11519 Prague 1, Czech Republic*

[17]*Institute of Physics and Technology, University of Bergen, Alleegaten 55, 5007 Bergen, Norway*

[18]*Institute for Nuclear Research of the Russian Academy of Science, Moscow 117312, Russia*

[19]*Department of Physics, University of Oslo, Semælands vei 24, 0371 Oslo, Norway*

[20]*Stefan Meyer Institute for Subatomic Physics, Austrian Academy of Sciences, Boltzmanngasse 3, 1090 Vienna, Austria*

[21]*Joint Institute for Nuclear Research, 141980 Dubna, Russia*

[22]*Istituto Nazionale di Fisica Nucleare Padova, via Marzolo 8, 35131 Padova, Italy*

[23]*Institute of Nuclear Physics, Centre National de la Recherche Scientifique/IN2p3, University of Lyon 1, 69622 Villeurbanne, France*

[24]*University of Bologna, Viale Berti Pichat 6/2, 40126 Bologna, Italy*

[25]*Department of Physics, University of Pavia, via Bassi 6, 27100 Pavia, Italy*

[26]*Department of Physics, University of Napoli Federico II, Complesso Universitario di Monte S. Angelo, 80126 Napoli, Italy*

[27]*The Research Council of Norway, Post Office Box 564, NO-1327 Lysaker, Norway*

[28]*Department of Civil Engineering, University of Brescia, via Branze 43, 25123 Brescia, Italy*

(Received 25 September 2015; revised manuscript received 31 May 2016; published 7 July 2016)

We demonstrate the laser excitation of the $n = 3$ state of positronium (Ps) in vacuum. A combination of a specially designed pulsed slow positron beam and a high-efficiency converter target was used to produce Ps. Its annihilation was recorded by single-shot positronium annihilation lifetime spectroscopy. Pulsed laser excitation of the $n = 3$ level at a wavelength $\lambda \approx 205$ nm was monitored via Ps photoionization induced by a second intense laser pulse at $\lambda = 1064$ nm. About 15% of the overall positronium emitted into vacuum was excited to $n = 3$ and photoionized. Saturation of both the $n = 3$ excitation and the following photoionization was observed and explained by a simple rate equation model. The positronium's transverse temperature was extracted by measuring

the width of the Doppler-broadened absorption line. Moreover, excitation to Rydberg states $n = 15$ and 16 using $n = 3$ as the intermediate level was observed, giving an independent confirmation of excitation to the $3\,^3P$ state.

DOI: 10.1103/PhysRevA.94.012507

I. INTRODUCTION

Positronium (Ps) is a purely leptonic hydrogenlike bound state composed of an electron (e^-) and its antiparticle, the positron (e^+). Its long-lived $1\,^3S$ state (ortho-positronium, o-Ps) predominantly annihilates into three photons with a lifetime of 142 ns in vacuum. Since the discovery of Ps in 1951 [1], it has become a prime testing ground of bound-state QED [2]. Up to now, the first excited state $n = 2$ and the Rydberg levels $n = 10$–31 have been experimentally observed [3–8]. Laser excitation of o-Ps has proven to be a very useful spectroscopic tool [9]; it also allows us to study or modify Ps formation [10,11], and to prepare selected states for further manipulation [8,12,13].

Ps also has been identified as a promising intermediate system for antihydrogen production via a charge-exchange reaction with an antiproton [14–19]. Specifically, laser excitation of Ps is of interest for antimatter gravity experiments. The GBAR (Gravitational Behavior of Antihydrogen at Rest) experiment, for example, plans to create positive antihydrogen ions by projecting slow Ps through a cloud of cold antiprotons [20,21]. This charge-exchange process is expected to benefit by exciting Ps to the $n = 3$ level [22–24]. A further remarkable increase (according to a cross-section power law proportional to n^4) is expected, exciting Ps to Rydberg states [15,16] with a two-step pathway that has been observed and well demonstrated using $n = 2$ as an intermediate step [6,8]. The AEgIS experiment is pursuing an alternative scheme, using $n = 3$ as an intermediate step to excite Ps Rydberg states [19,25], as measured for the first time in the present work.

Moreover, excitation of the Ps $n = 3$ level can be an efficient pathway for producing a beam of metastable $2\,^3S$ Ps atoms by spontaneous decay. In fact, the theoretical prediction for the ratio of the spontaneous emission rates $(3\,^3P \rightarrow 2\,^3S)/(3\,^3P \rightarrow 1\,^3S)$ is 13.4% [26]. Experimentally, it has been demonstrated that in the hydrogen system the branching ratio from $n = 3$ to $2\,^3S$ is about 12% [27]. Using scaling considerations between hydrogen atom and the hydrogeniclike Ps, their branching factors are expected to be identical. This makes the production of the $n = 2$ metastable state using $n = 3$ as the intermediate level a potentially interesting alternative to other methods, for instance, two-photon laser induced transition from $1\,^3S$ to $2\,^3S$, which has been realized in various configurations, both pulsed [4] and continuous [28]. This could open the way to high-precision measurements of the $1\,^3S$-$2\,^3S$ transition [28] and interferometry experiments with long-lived Ps beams [13].

In this work we demonstrate an efficient excitation of the $n = 3$ level in Ps. For this purpose, we used a pulsed laser system that was developed with the aim of efficiently saturating the $1\,^3S$-$3\,^3P$ transition [29] in the cryogenic and high-magnetic-field environment of the AEgIS main trap, in which antihydrogen formation is planned to occur [19]. To fulfill this requirement the laser was developed with a bandwidth able to cover the Doppler broadening and most of the motional Stark mixing of the transition.

II. EXPERIMENTAL

The present experiment was performed in a chamber in which Ps annihilations were monitored using the single-shot e^+ annihilation lifetime spectroscopy (SSPALS) technique [30,31]. The population of the $n = 3$ level was independently confirmed by photoionization and by the excitation of Rydberg levels using a second laser. The experimental setup is described in detail in Refs. [32,33]. Briefly, positrons emitted by a 11 mCi ^{22}Na source were slowed down by a solid Ne moderator [34] and then prepared by a Surko-style trap [35] and accumulator. After rotating-wall compression [36], 20-ns bunches containing 3×10^7 positrons each were produced by fast-switched electric potentials and transported to a magnetic-field-free region. There they were recompressed [37] with a 24-electrode buncher [33] into a pulse of about 7 ns and accelerated onto a nanochanneled silicon target with a kinetic energy of 3.3 keV. In the target, e^+ are efficiently converted into o-Ps and emitted into vacuum [38,39]. Using a calibrated CsI detector and a microchannel plate (MCP) with a phosphor screen in place of the silicon target, it was estimated that 30–40% of positrons released from the accumulator hit the sample in a spot of < 4 mm full width at tenth of maximum (FWTM). Two symmetric coils allow tuning of a longitudinal magnetic field in the sample region to induce o-Ps quenching [3,40–42]. All experiments were performed in a 600-V/cm electric- and 0.025-T magnetic-field environment, with the magnetic field perpendicular to the target, which was kept at room temperature.

A $20 \times 25 \times 25$-mm lead tungstate ($PbWO_4$) scintillator [31] coupled to a Hamamatsu R11265-100 photomultiplier tube (PMT) was placed 40 mm above the sample to record γ rays emitted in positron-electron annihilations. The geometry of the Ps production region with the distances of the target from the walls of the chamber is shown in Fig. 1. To enhance resolution at the longest decay times, the signal from the PMT was split and sent to two channels of a 500-MHz oscilloscope with high (100 mV/division) and low (1 V/division) gain. Joined data from the two channels give the SSPALS spectra shown in Fig. 2 when e^+ are bunched on the surface of the MCP (no Ps formation; background) and on the target (Ps formation).

*Corresponding author: Sebastiano.Mariazzi@cern.ch

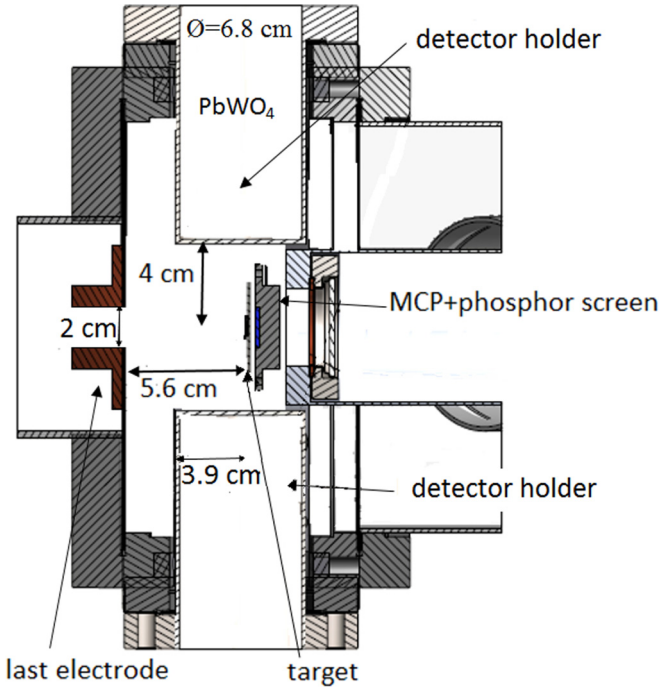

FIG. 1. Sketch of the Ps production region with the distances of the target from the walls of the chamber and the detector holders. The position of the $PbWO_4$ scintillator used for SSPALS measurements is reported. In the present work the "detector holder" on the bottom part of the figure was used to make the chamber symmetric.

The laser setup is described in detail in Ref. [29]. The first laser system was able to deliver 54-μJ pulses of UV light to the experimental room-temperature chamber, in a wavelength range 204–206 nm. The wavelength was tuned by adjusting the temperature of an optical parametric generator crystal.

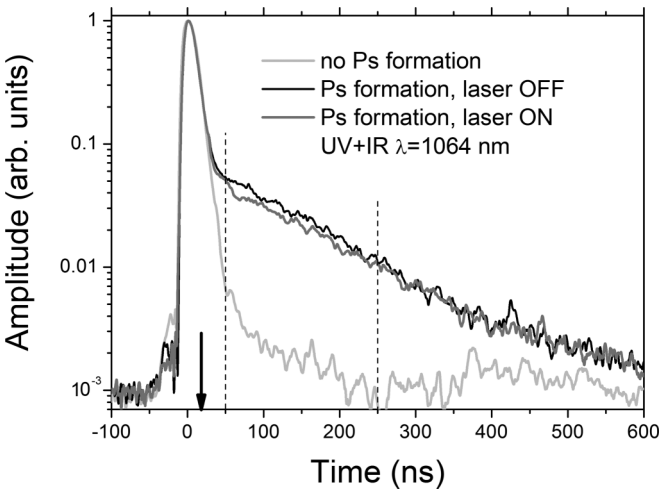

FIG. 2. SSPALS spectra of background in light gray line, Ps into vacuum with laser OFF in black and UV+IR lasers ON (205.05 + 1064 nm) in dark gray. Each spectrum is the average of 15 single shots. The arrow marks the time when the laser is shot on the Ps cloud (16 ns after prompt peak). The area between 50 and 250 ns from the prompt peak (vertical dashed lines) was used to evaluate S for $n = 3$ (see text).

The pulse has a horizontal polarization, i.e., perpendicular to the sample (see Fig. 1); an asymmetric, nearly Gaussian temporal profile with a full width at half maximum (FWHM) of $t_{UV} \approx 1.5$ ns; a Gaussian-like spectral profile with $\sigma_{laser} \approx 2\pi \times 48$ GHz; and a slightly elliptical Gaussian spatial shape, with $FWHM_{vertical} = 6$ mm and $FWHM_{horizontal} = 4$ mm [43]. A second, intense IR laser pulse at 1064 nm was simultaneously delivered to the experimental chamber. This horizontally polarized pulse has an energy of 50 mJ and a temporal FWHM of 10 ns. It was superimposed on the 205-nm pulse both in time, with a precision of 1 ns using an optical delay line, and in space, by increasing its size so as to completely cover the excitation pulse area (top-hat profile of 8-mm diameter). Both beams were aligned on the target region by monitoring their position with a CCD camera on a 1-in. Macor screen placed inside the vacuum region, a few cm away from the target. A mutual synchronization of positrons and laser pulses with a time resolution of 2 ns and a jitter of less than 600 ps was obtained by a custom field-programmable gate array based synchronization device. The time delay between the prompt positron annihilation peak and the laser pulses was set to 16 ns (vertical arrow in Fig. 2).

III. RESULTS AND DISCUSSION

The fraction of excited o-Ps was measured by analyzing the decrease in the annihilation rate in the SSPALS spectra induced by populating the $3\,^3P$ state. Two methods can be used for this purpose: (i) quenching in a magnetic field or (ii) photoionization with the IR laser pulse. In the absence of a magnetic field, $3\,^3P$ states decay radiatively to the $1\,^3S$ state in 10.5 ns. In presence of a magnetic field, (i) the $3\,^3P$ substates with $m = 0, \pm 1$ (excluding $3\,^3P_{10}$) are mixed with the $3\,^1P$ substates [26], and can decay toward the $1\,^1S$ state, subsequently annihilating with a lifetime of 125 ps into two γ rays; otherwise, (ii) photoionization of the $3\,^3P$ state dissociates the Ps and the free positrons are quickly accelerated toward the last negative electrode of our setup, where they annihilate. Whichever technique is chosen, both processes result in a decrease of the o-Ps population decaying into three γs. The fraction of excited o-Ps can be evaluated by analyzing the decrease in the area below the SSPALS spectra when quenching or photoionization are applied. The fraction S of quenched or ionized o-Ps atoms was evaluated from the areas f_{off} and f_{on} of the SSPALS spectra, with UV laser (or UV+IR lasers) off and on, between 50 and 250 ns from the prompt peak: $S = (f_{off} - f_{on})/f_{off}$.

To predict the value of the external field required to get the maximum magnetic quenching efficiency, we used a simulation code which performs the numerical diagonalization of the full interaction Hamiltonian in arbitrary electric and magnetic fields and calculates the generalized Einstein coefficients and sublevel lifetimes. These coefficients were fed into a rate equation solver [26] to study the complex excitation dynamics of Ps considered as an incoherent process induced by the UV laser pulse at resonance, and assuming ideal conditions (exact superposition of the UV laser bandwidth on Ps Doppler linewidth, perfect temporal and geometrical overlap). According to simulation results, we obtain the maximum quenching efficiency of 17% on the $n = 3$ excitation

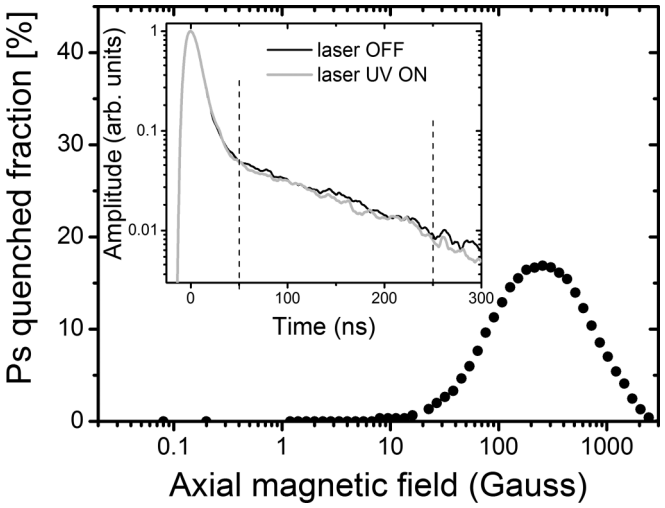

FIG. 3. Simulated quenching efficiency vs axial magnetic field. Inset: SSPALS spectra of Ps into vacuum with laser OFF in black and UV laser ON (205.05 nm) in light gray measured at 250 Gauss. Each spectrum is the average of 15 single shots. The vertical dashed lines mark the area used to evaluate the S parameter (see text).

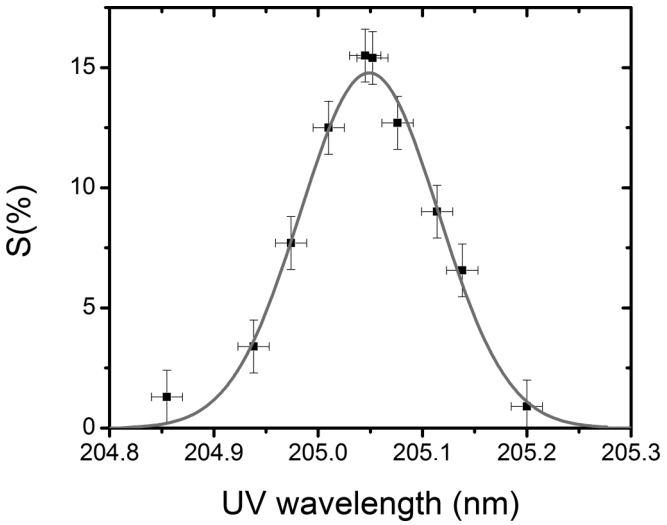

FIG. 4. Linewidth of the $1\,^3S$-$3\,^3P$ Ps excitation obtained by scanning the UV laser wavelength for constant IR wavelength. Each point has been calculated by averaging 15 SSPALS spectra. Statistical errors (on the y axis) and accuracy (on the x axis) are reported (see text). The continuous line is a fit obtained with Eq. (3).

with a 0.025-T magnetic field in the sample region (Fig. 3). The results were largely independent of the Ps velocity. Similar simulations were performed to predict the total efficiency of the excitation+ionization processes, in the case of the superposition of the IR laser pulse, obtaining ∼93% with our laser parameters.

We then set a 0.025-T magnetic field in the sample region and measured the quenching efficiency following the $n = 3$ excitation. The SSPALS spectra obtained in this experiment are reported in the inset of Fig. 3 showing a small reduction of o-Ps annihilations in the selected S window when the UV laser is on. The maximum observed reduction through quenching was $S = 3.6 \pm 1.2\%$. When applying the IR pulse for photoionization, the decrease in o-Ps annihilations becomes plainly visible in the SSPALS spectrum of Fig. 2, corresponding to $S = 15.5 \pm 1.1\%$. The ratio of the experimental to the theoretical efficiencies are $3.6/17 \approx 0.21$ and $15.5/93 \approx 0.17$, for quenching and ionization, respectively. The two ratios are in reasonable agreement with each other, indicating that our experimental efficiency is around 17–21% of the maximum theoretical one. In our experimental setup, the main limitations are due to the limited laser spectral width, that does not cover the entire Doppler profile of Ps emitted from a room-temperature target, and the limited geometrical overlap of the laser spot on the Ps cloud (see below).

We scanned the UV wavelength using an Avantes AvaSpec-3648-USB2 wavemeter (accuracy $= \pm 0.02$ nm). At each wavelength, the mean S value and its standard deviation were calculated for a sample of 15 shots (Fig. 4).

Fitting a Gaussian to the resulting points gives the central value of the $3P$ excitation line at 205.05 ± 0.02 nm. The value predicted by theory is 205.0474 nm [26]. The saturation energies of both $1S$-$3P$ and $3P$-ionization transitions have been studied (see Fig. 5). The $1S$-$3P$ transition appears only slightly saturated, while the $3P$ continuum is strongly saturated, meaning that almost all of the $n = 3$ atoms are photoionized as soon as they are excited. Thus, the S value found when photoionizing can directly be seen as the excitation efficiency. From our data we conclude that $\approx 15\%$ of the overall positronium emitted in vacuum has been excited into the $n = 3$ state, and subsequently photoionized.

To analyze these results, we used a simple three-level rate equation model, which neglects spontaneous emission and assumes that the laser pulses are constant over the pulse time t. At strong IR intensities the $n = 3$ states are very quickly photoionized. This leads to a probability for Ps($n = 3$) photoionization [44]:

$$p(t,\mathbf{r},\mathbf{v},\delta) = 1 - e^{-\gamma t}, \tag{1}$$

where γ is the UV absorption rate. Our laser spectrum has a linewidth σ_{laser} much larger than the ionization rate and of both the natural linewidth and the hyperfine splitting structure

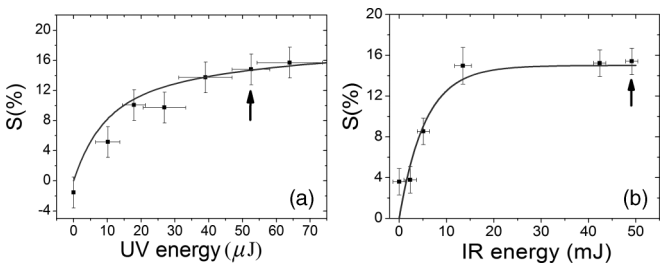

FIG. 5. S parameter (as defined in the text) as a function of UV energy (IR energy = 50 mJ) (a) and IR energy (UV energy = 54 μJ) (b). Arrows mark the laser energies used for the measurements of Fig. 4. The continuous lines are fits of the three-level rate equation model (see text).

(3 GHz), hence

$$\gamma(\mathbf{v},\mathbf{r},\delta) \approx \frac{\pi\Omega^2(\mathbf{r})}{2}\frac{1}{\sqrt{2\pi\sigma^2_{\text{laser}}}}e^{-(\delta-\mathbf{k}\cdot\mathbf{v})^2/2\sigma^2_{\text{laser}}}, \qquad (2)$$

where δ is the laser frequency detuning with Ps at rest ($\mathbf{v}$ being the Ps velocity), $\mathbf{k}$ is the UV laser wave number, and $\Omega(\mathbf{r})$ is the Rabi frequency that depends on the position $\mathbf{r}$ of the Ps in the laser beam. Spatial averaging with the (Gaussian) Ps density profile can then be performed.

For our moderate saturation, we found it more meaningful to extrapolate the spatial averaging result—valid at low saturation (where $p \approx \gamma t$)—by defining a geometrical overlapping efficiency coefficient η, and thus Ω is replaced by its peak value. The probability of photoionization, assuming a Ps cloud at temperature T, is then given by

$$P(t,\delta) = \eta\int_{-\infty}^{+\infty} p(t,v,\delta)\sqrt{\frac{1}{2\pi\sigma_v^2}}e^{-\frac{v^2}{2\sigma_v^2}}\,dv, \qquad (3)$$

where $\sigma_v = \sqrt{k_B T/m}$ is the standard deviation of the velocity along the laser propagation axis. This formula was used to fit the data in Figs. 4 and 5(a). We find $\Omega^2 = 8\times10^{10}\,\text{s}^{-1}\times\frac{E_{\text{UV}}}{t_{\text{UV}}}$, where E_{UV} is the energy of the 205 nm laser, in μJ, and t_{UV} the pulse length in seconds. This corresponds to a dipole strength $d = 1.70$ D, in good agreement with the theoretical value of 1.65 D predicted in Ref. [25].

The line shape of Fig. 4 is almost entirely dominated by the thermal distribution of the Ps, so we obtain a standard deviation of o-Ps velocity in the transverse direction $\sigma_v \approx 10^5$ m/s, or a temperature $T \approx 1300$ K.

The Ps transverse velocity component observed in the present experiment is in the same range of the mean longitudinal velocity component observed in the experiments of Refs. [39,45]. Both measurements have been carried out using nanochanneled silicon samples with similar nanochannels size. This finding can be explained by two concurrent effects. The first could be ascribed to the different orientation of the produced nanochannels: samples of Refs. [39,45] were produced by etching Si p-type crystals (100) oriented, while the sample used for the present measurement was produced by etching Si p-type crystals (111) oriented. In the first case nanochannels are expected to be rather perpendicular to the surface, while in the second case they are expected to form a network at 45° with respect to the surface (see, for example, Ref. [46]). The second effect could be due to a randomization of the Ps trajectories escaping into vacuum after the collision with the irregular walls of the nanochannels. From the scanning electron microscope images reported in Ref. [39], it is evident that the outlets of the nanochannels are very "rough" on a microscopic scale, with different orientation of their surfaces. The last collisions of Ps could indeed produce as final effect an extremely wide angle of emission. Finally, a more isotropic emission could be expected at low positron implantation energies (i.e., more Ps formation near the surface) as in the present experiment.

According to the previously described fitting procedure, we also find a large geometrical overlap $\eta \approx 80\%$.

Considering that the laser bandwidth is $\sigma_{\text{laser}} = 2\pi\times 48$ GHz and the total Doppler broadened Ps linewidth is $k\sigma_v \approx 2\pi\times 470$ GHz, one should expect to reach an excitation efficiency up to 10% because of the convolution of the two spectral distributions. This confirms that the main limitation for efficient Ps excitation comes from the limited laser bandwidth compared to the Doppler profile.

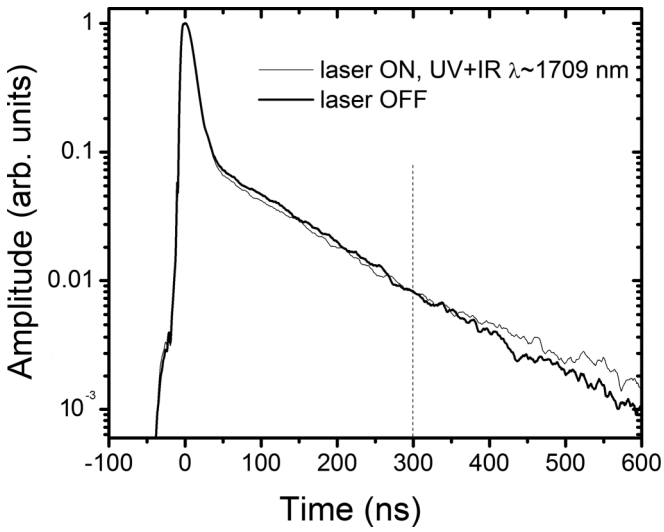

FIG. 6. SSPALS spectra of Ps into vacuum with UV+IR lasers OFF in black, and laser UV+IR ON (205.05 + 1709 nm) in dark gray. Shown spectra are composed by averaging 40 single shots. Area between 300 ns (vertical dashed line) and 600 ns from the prompt peak has been considered for evaluation of S for Rydberg levels (see text).

Finally we used the rate equation model to fit the data in Fig. 5(b) and found a maximum ionization rate of 5.0×10^9 s^{-1}, corresponding to a photoionization cross section by the IR photons of $\approx 3.1\times10^{-17}$ cm^2, in good agreement with the theoretical value of $\approx 3.5\times10^{-17}$ cm^2.

An independent test to demonstrate the excitation of the $3\,^3P$ level was performed with an IR laser pulse suitable for exciting Ps to Rydberg levels. A first demonstration of Rydberg excitation using $3\,^3P$ as the intermediate level was carried out by simply varying the wavelength of the IR pulse. Rydberg excitation increases the o-Ps lifetime, allowing a large number of o-Ps to reach the walls of the vacuum chamber. As a consequence, the SSPALS spectra show a decrease of annihilations immediately after the laser shot and an increase at later times (Fig. 6) [47]. In our experimental system, around 30% of the walls of the chamber reached by Ps atoms are between 4 and 6 cm far from the target (see Fig. 1). Assuming a Ps velocity of the order of 10^5 m/s, the annihilation of Ps with the walls is expected to take about 400–600 ns. This time is consistent with the increase of annihilations observed in Fig. 6.

A scan of the IR laser wavelength was carried out in order to excite Ps from $n = 3$ to levels between $n = 15$ and 18, while the UV laser was kept on the resonance with the $n = 1 \rightarrow n = 3$ transition ($\lambda = 204.05$ nm, $E = 54\,\mu$J). The IR pulse energy was kept constant during the scan at $E = 1.1\pm0.1$ mJ. The Rydberg excitation signal was extracted from the SSPALS spectra by calculating the S parameter in the time window between 300 and 600 ns after the prompt positron annihilation peak.

The wavelength of the IR pulse was measured at the beginning of each set of 15 measurements, corresponding to one data point. To do so, a 1-cm lithium niobate doubling crystal was inserted in the laser line to send the second harmonic generated into a commercial Thorlabs CCS175 spectrometer, having a spectral range 500–1000 nm. In the range 1650–1720 nm, the doubling crystal has an acceptance bandwidth of $2\pi\times$ 800–1000 GHz, much broader than the bandwidth of the IR pulse ($\sigma_{\rm IR} = 2\pi\times$ 48–106 GHz, depending on the mutual optical parametric amplifier (OPA) crystals alignment). The phase-matching angle of the crystal was optimized for each wavelength of the scan by maximizing the outgoing beam intensity, in order to avoid systematic effects related to a limited crystal acceptance angle. The CCS175 spectrometer was used during the data taking with its original factory calibrations. At the end of the measurement campaign, a spectrum of a mercury lamp was acquired with high statistics, using the same set of calibration coefficients. Five mercury lines in the range 541–707 nm were clearly identified. Together with the theoretical position of the first two YAG lines (531.91 and 1064.82 nm), these Hg peaks were used to fit a linear model to the NIST reference values for mercury in air [48]. A shift in the measured wavelengths in the range 532–1064 nm versus the reference NIST lines of 1.14 ± 0.86 nm was observed, while on the contrary the angular coefficient of the spectrometer was found compatible with unity within the statistical sensitivity. The statistical uncertainty for a single measurement in this wavelength range was found to be very close to the spectrometer specifications (0.57 nm measured versus 0.6 nm declared by manufacturer), even if its resolution of 6 px/mm would suggest a higher accuracy.

The IR laser spectrum is slightly asymmetric around the peak wavelength, due to different phase-matching angles of the OPA crystals. We corrected the data according to the linear model obtained from the calibration and considered the intensity-weighted average of the spectrum as central wavelength. This choice is motivated by the narrow IR laser bandwidth ($\sigma_{\rm IR} = 2\pi\times$ 48–106 GHz) compared to the observed $k\sigma_v \approx 2\pi\times$ 470-GHz linewidth of the $n = 3$ state. We expect the $n = 15$ level to be even more broadened than the $n = 3$ one, due to the added contribution from the motional Stark effect [49], almost negligible for low excited states.

Despite this significant broadening of the Rydberg lines, we observed the $n = 15$ transition clearly isolated; for higher states, different n manifolds start to overlap in a continuum of energy levels [49]. This is shown in Fig. 7, which reports experimental data together with a Gaussian fit of the Rydberg $n = 15$ line. The resulting peak wavelength has been determined to be 1710.0 ± 0.6 nm.

Contrary to the spectroscopic survey carried out in Ref. [8], our experiment is performed in a 600-V/cm electric field. The zero-field excitation line central value for $n = 15$ is expected to be 1708.63 nm; hence our experimental data show a line shift of around 1.4 nm towards higher wavelengths, about ten times greater than the shift that can be evaluated by the presence of quadratic Stark effects.

The reason underlying this notable line shift is under investigation; a first suggested interpretation involves a dynamical feature provoking an uneven distribution of the exciting lines in arbitrary external electric fields, due to uneven dipole strengths of the transitions, for our electric- and magnetic-field conditions. This will be the topic of a future dedicated study [50].

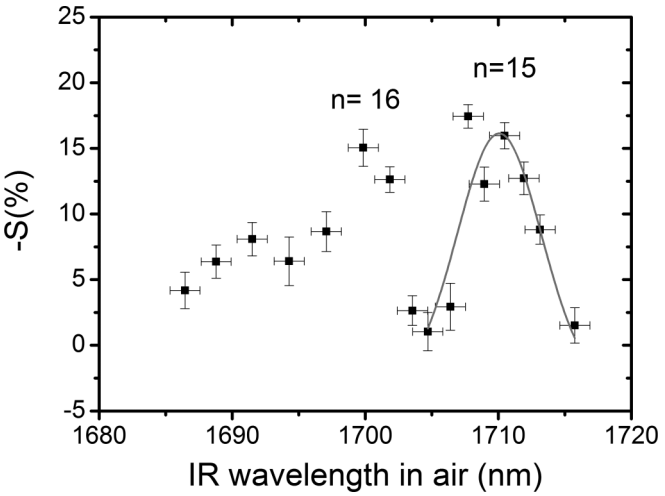

FIG. 7. Scan of the S parameter as defined in the test vs the IR wavelength in air in the range $n = 15$–18. The clearly identifiable peak, associated to the transitions to $n = 15$, has been fitted with a Gaussian. For $n > 16$, lines are no more clearly separated due to the excessive broadening.

IV. SUMMARY

In the present work, we have demonstrated the laser excitation of Ps to the $n = 3$ state. The total excitation+photoionization efficiency of $\approx 15\%$ is mainly limited by the ratio of the laser linewidth to the Doppler broadening of the Ps line. Reduction of the o-Ps emission velocity from the target is thus an obvious way to enhance the excitation efficiency. An excitation to Rydberg levels using $3\,^3P$ as the intermediate state has also been shown, opening the possibility for further studies involving $n = 3 \longrightarrow$ Rydberg transitions [49]. Hence, the production of Ps in the $n = 3$ level opens the way to many intriguing research subjects, ranging from the study and manipulation of long-lived exotic atoms to the production of ultracold antimatter.

ACKNOWLEDGMENTS

This work was supported by Istituto Nazionale di Fisica Nucleare; a Deutsche Forschungsgemeinschaft research grant; an excellence initiative of Heidelberg University; European Research Council under the European Unions Seventh Framework Program FP7/2007-2013 (Grants No. 291242 and No. 277762); Austrian Ministry for Science, Research, and Economy; Research Council of Norway; Bergen Research Foundation; John Templeton Foundation; Ministry of Education and Science of the Russian Federation and Russian Academy of Sciences; and the European Social Fund within the framework of realizing the project, in support of intersectoral mobility and quality enhancement of research teams at Czech Technical University in Prague (Grant No. CZ.1.07/2.3.00/30.0034).

[1] M. Deutsch, Phys. Rev. **82**, 455 (1951).
[2] S. G. Karshenboim, Phys. Rep. **422**, 1 (2005).
[3] K. P. Ziock, C. D. Dermer, R. H. Howell, F. Magnotta, and K. M. Jones, J. Phys. B **23**, 329 (1990).
[4] S. Chu and A. P. Mills, Phys. Rev. Lett. **48**, 1333 (1982).
[5] K. P. Ziock, R. H. Howell, F. Magnotta, R. A. Failor, and K. M. Jones, Phys. Rev. Lett. **64**, 2366 (1990).
[6] D. B. Cassidy, T. H. Hisakado, H. W. K. Tom, and A. P. Mills, Phys. Rev. Lett. **108**, 043401 (2012).
[7] A. C. L. Jones, T. H. Hisakado, H. J. Goldman, H. W. K. Tom, A. P. Mills, and D. B. Cassidy, Phys. Rev. A **90**, 012503 (2014).
[8] T. E. Wall, A. M. Alonso, B. S. Cooper, A. Deller, S. D. Hogan, and D. B. Cassidy, Phys. Rev. Lett. **114**, 173001 (2015).
[9] D. B. Cassidy, T. H. Hisakado, H. W. K. Tom, and A. P. Mills, Phys. Rev. Lett. **109**, 073401 (2012).
[10] D. B. Cassidy, M. W. J. Bromley, L. C. Cota, T. H. Hisakado, H. W. K. Tom, and A. P. Mills, Phys. Rev. Lett. **106**, 023401 (2011).
[11] D. B. Cassidy, T. H. Hisakado, H. W. K. Tom, and A. P. Mills, Phys. Rev. Lett. **106**, 133401 (2011).
[12] M. Becucci, G. Ferrari, I. Boscolo, F. Castelli, S. Cialdi, F. Villa, and M. Giammarchi, J. Mol. Struct. **993**, 495 (2011).
[13] D. B. Cassidy and S. D. Hogan, Int. J. Mod. Phys.: Conf. Ser. **30**, 1460259 (2014).
[14] M. Charlton, F. M. Jacobsen, and B. I. Deutch, J. Phys. B **20**, L25 (1987).
[15] M. Charlton, Phys. Lett. A **143**, 143 (1990).
[16] M. Charlton, J. Eades, D. Horváth, R. Hughes, and C. Zimmermann, Phys. Rep. **241**, 65 (1994).
[17] E. A. Hessels, D. M. Homan, and M. J. Cavagnero, Phys. Rev. A **57**, 1668 (1998).
[18] C. H. Storry *et al.* (ATRAP Collaboration), Phys. Rev. Lett. **93**, 263401 (2004).
[19] M. Doser *et al.* (AEgIS Collaboration), Class. Quantum Grav. **29**, 184009 (2012).
[20] P. Perez and Y. Sacquin, Class. Quantum Grav. **29**, 184008 (2012).
[21] P. Perez *et al.* (GBAR Collaboration), Hyperfine Interact. **233**, 21 (2015).
[22] P. Comini and P.-A. Hervieux, New J. Phys. **15**, 095022 (2013).
[23] P. Comini, P.-A. Hervieux, and F. Biraben, Hyperfine Interact. **228**, 159 (2014).
[24] A. S. Kadyrov, C. M. Rawlins, A. T. Stelbovics, I. Bray, and M. Charlton, Phys. Rev. Lett. **114**, 183201 (2015).
[25] F. Castelli, I. Boscolo, S. Cialdi, M. G. Giammarchi, and D. Comparat, Phys. Rev. A **78**, 052512 (2008).
[26] F. Villa, Laser system for positronium excitation to Rydberg levels for Aegis experiment, Ph.D. Thesis, Universitá degli studi di Milano, 2011.
[27] K. C. Harvey, J. Appl. Phys. **53**, 3383 (1982).
[28] D. Cooke, P. Crivelli, J. Alnis, A. Antognini, B. Brown, S. Friedreich, A. Gabard, T. Haensch, K. Kirch, A. Rubbia, and V. Vrankovic, Hyperfine Interact. **233**, 67 (2015).
[29] S. Cialdi, I. Boscolo, F. Castelli, F. Villa, G. Ferrari, and M. Giammarchi, Nucl. Instrum. Methods Phys. Res. B **269**, 1527 (2011).
[30] D. B. Cassidy, S. H. M. Deng, H. K. M. Tanaka, and A. P. Mills, Appl. Phys. Lett. **88**, 194105 (2006).
[31] D. B. Cassidy and A. P. Mills, Nucl. Instrum. Methods Phys. Res. A **580**, 1338 (2007).
[32] L. Penasa, L. Di Noto, M. Bettonte, S. Mariazzi, G. Nebbia, and R. S. Brusa, J. Phys.: Conf. Ser. **505**, 012031 (2014).
[33] S. Aghion *et al.* (AEgIS Collaboration), Nucl. Instrum. Methods Phys. Res. B **362**, 86 (2015).
[34] A. P. Mills and E. Gullikson, Appl. Phys. Lett. **49**, 1121 (1986).
[35] J. R. Danielson, D. H. E. Dubin, R. G. Greaves, and C. M. Surko, Rev. Mod. Phys. **87**, 247 (2015).
[36] R. G. Greaves and C. M. Surko, Phys. Rev. Lett. **85**, 1883 (2000).
[37] A. P. Mills, Appl. Phys. **22**, 273 (1980).
[38] S. Mariazzi, P. Bettotti, S. Larcheri, L. Toniutti, and R. S. Brusa, Phys. Rev. B **81**, 235418 (2010).
[39] S. Mariazzi, P. Bettotti, and R. S. Brusa, Phys. Rev. Lett. **104**, 243401 (2010).
[40] S. M. Curry, Phys. Rev. A **7**, 447 (1973).
[41] A. Rich, Rev. Mod. Phys. **53**, 127 (1981).
[42] A. Deller, D. Edwards, T. Mortensen, C. A. Isaac, D. P. van der Werf, H. H. Telle, and M. Charlton, J. Phys. B **48**, 175001 (2015).
[43] R. Caravita, Laser apparatus for exciting Positronium in AEGIS Positronium spectroscopy experiment, Masters Thesis, University of Milano, 2012.
[44] R. Horchani, Optical pumping of cesium molecules: vibrational cooling and electronic conversion, Ph.D. Thesis, Université Paris Sud—Paris XI, 2011.
[45] S. Mariazzi, L. Di Noto, G. Nebbia, and R. S. Brusa, J. Phys.: Conf. Ser. **618**, 012039 (2015).
[46] S.-F. Chuang, S. D. Collins, and R. L. Smith, Appl. Phys. Lett. **55**, 675 (1989).
[47] The different signal to noise ratio of the laser off curves reported in Figs. 2 and 6 is due to the different statistics and the slightly different number of positrons in the accumulator due to the fringe magnetic fields generated by the antiproton decelerator ring of CERN. In order to preserve the relative line-shape difference between the laser on and off curves and to avoid any impact on the estimation of the S parameter due to possible drifts of the experimental conditions, we alternated measurements with laser on and off.
[48] A. Kramida, Yu. Ralchenko, J. Reader, and NIST ASD Team, NIST Atomic Spectra Database, Ver. 5.3, http://physics.nist.gov/PhysRefData/Handbook/Tables/mercurytable2.html [25 May 2016], National Institute of Standards and Technology, Gaithersburg, MD, 2015.
[49] F. Castelli, Eur. Phys. J. Special Topics **203**, 137 (2012).
[50] R. Caravita and F. Castelli (unpublished).